An Optimized Combined Wave and Current Algorithm for Arbitrary Bed Roughness

Richard Styles
Department of Geological Sciences and Marine Science Program, University of South Carolina, Columbia, South Carolina, 29208, USA

Scott M. Glenn
Institute of Marine and Coastal Sciences, Rutgers University, New Brunswick, New Jersey, 08901, USA

Technical Report
Boundary Layer Stress and Sediment Transport Laboratory, Department of Geological Sciences, University of South Carolina

December 2002

Table of Contents:

Abstract

A generalized method for computing the bed shear stress in unstratified combined wave and current flows is presented. The present approach follows from existing theories describing the nonlinear wave and current interaction in the benthic boundary layer, but is designed for arbitrary wave, current and roughness conditions, including the limiting case of pure waves or pure currents. The stress model is intended for use with 3-dimensional shelf circulation models, where a broad range of flow conditions are encountered. Model results indicate that for moderately rough conditions, the form of the eddy viscosity outside the wave boundary layer has little effect on the value of the bed stress. For very rough beds, the form of the eddy viscosity is important and must be accurately resolved. High-quality data for combined flows and pure waves are used with the present stress formulation to better refine empirical model closure constants in the fully rough turbulent regime. Introducing a first order correction to the definition of the wave boundary layer thickness produces accurate estimates of both the measured friction factor and wave boundary layer height. A speed of convergence test indicates that the present model is significantly more efficient than previous models that use the same turbulent closure scheme. This is primarily due to an improved solution algorithm that avoids the nested iterations common to established combined wave and current bottom boundary layer models.

1.0 Introduction

An important physical process for coastal circulation modeling is the interaction in the bottom boundary layer between waves and currents and how these both interact with the bottom to modify bedforms and move sediment. A very important result of wave-current interaction theorized over two decades ago is the enhancement of the current shear stress due to waves (Smith 1977; Grant and Madsen 1979). Repeated measurements on storm-dominated shelves have illustrated that nonlinear wave-current interaction can significantly enhance the roughness of the bed and the stress felt by the current (e.g., Cacchione and Drake 1982; Wiberg and Smith 1983; Grant et al. 1984; Drake et al. 1992). Therefore, wave-current interaction is expected to play a dominant role in the momentum balance of low frequency shelf motion and should be considered in any realistic modeling effort in storm-dominated shelf regions. This is especially important if one of the primary purposes is to study shallow water sediment transport.

Modeling studies of shelf circulation patterns that incorporate wave-current effects in the bottom boundary layer have been conducted in the past (e.g., Spaulding and Isaji 1985; Cooper and Thompson 1989; Signell et al. 1990; Davies and Lawrence 1993; Keen and Slingerland 1993a, b; Keen and Glenn 1994; Keen and Glenn 1995). Keen and Glenn (1994) provide a brief summary of coupled and uncoupled versions of the Grant and Madsen (1979) (hereinafter referred to as GM) and Glenn and Grant (1987) bottom boundary layer models (BBLMs) implemented in shelf circulation models. Their review identifies a number of responses directly related to enhanced bottom shear stress due to waves on continental shelves including a reduction in current speed near the bottom, modification of sediment transport rates, and enhanced turning of the current vector in the bottom Ekman layer that increases upwelling and downwelling. Keen and Glenn (1995) also showed increased offshore rotation of the current vector during downwelling, and reduction in bottom current speeds in shallow water in a simulation of storm and tidal flow in the Middle Atlantic Bight. More recently, Keen and Glenn (1998) carried out a quantitative skill assessment of model performance using moored current meter data from the Gulf of Mexico during Hurricane Andrew. One of the sensitivities they studied included a three order of magnitude variation in bottom roughness length; the largest roughness serving as a surrogate for the enhanced apparent bottom roughness known to occur in combined wave and current flows. Modeled currents showed the greatest sensitivity to bed roughness when compared to bottom currents measured in a water depth of 15 m. Normalized peak speed differences between measured and modeled currents decreased when the apparent roughness was increased from 0.1 cm to 10 cm. Because their model did not include wave-current interaction, the roughness and stress fields could not evolve in response to changing wave conditions. Even so, the higher correlation between modeled and measured currents in shallow water for simulated roughnesses comparable to that associated with the presence of surface waves reemphasizes the fact that wave-current effects are very important on storm-dominated continental shelves.

The above results of Keen and Glenn are based on a streamlined version of the GM wave and current BBLM (Keen and Glenn 1994). Like the original GM model, the streamlined version assumes that the roughness length is small compared to the wave boundary layer height, and that the height of the reference current needed to drive the model (usually the lowest grid point) is greater than the wave boundary layer height. For arbitrary roughness lengths and model grid heights, it is possible that under some conditions neither of these requirements will be met. The streamlined version also uses the discontinuous eddy viscosity adopted by GM and Glenn and Grant (1987), which has been shown to be less accurate than more physically reasonable continuous eddy viscosity profiles for combined flows (Glenn 1983; Madsen and Wikramanayake 1991; Lynch et al. 1997; Styles and Glenn 2000) and pure waves (Sleath 1991; Nielsen 1992; Davies and Villaret 1997).

Here we present a robust method for computing bottom stress in combined wave and current flows on the continental shelf that can be easily implemented as a subroutine in shelf circulation models. The model is basically an extension of the Styles and Glenn (2000) version of the GM model, but has been modified to incorporate arbitrary roughness configurations and a broader range of turbulence closure schemes (i.e., different eddy viscosity profiles). The approach adopted here is based on systematic scaling of the equations and careful selection of key non-dimensional parameters so that a closed solution can be formulated.

In the following section, the model formulation is described emphasizing the modifications required to extend the bottom stress theory to include very rough flow conditions. Model sensitivities to the eddy viscosity profile and a calibration of poorly constrained internal model closure constants is presented in Section 3. This is followed by a speed of convergence test, and the results are summarized in Section 4.

2.0 Model Formulation

The stress model developed here follows that of GM, in which the maximum combined shear stress, $\boldsymbol{\tau}_{cw}$, is written as the vector sum of the time averaged component associated with the current, $\boldsymbol{\tau}_c$, plus the maximum component associated with the wave, $\boldsymbol{\tau}_{wm}$,

$$\boldsymbol{\tau}_{cw} = \boldsymbol{\tau}_c + \boldsymbol{\tau}_{wm}, \tag{1}$$

where bold face denotes a vector quantity. Writing the stresses in terms of their respective shear velocities, $\boldsymbol{u}_* = (\tau/\rho)^{1/2}$, and taking the magnitude gives

$$u_{*cw}^2 = \sqrt{u_{*c}^4 + 2u_{*c}^2 u_{*wm}^2 \cos\phi_{cw} + u_{*wm}^4}\ , \tag{2}$$

where ρ is the fluid density and ϕ_{cw} ($0 \le \phi_{cw} \le \pi/2$) is the angle between the wave and current. To obtain a closed set of equations for the shear velocities, we adopt the usual gradient transport relation for the wave,

$$u_{*wm}^2 = \lim_{z \to z_0} \left(K \frac{\partial u_w}{\partial z} \right), \tag{3}$$

and for the current,

$$u_{*c}^2 = \lim_{z \to z_0} \left(K \frac{\partial U}{\partial z} \right), \tag{4}$$

where K is the time independent eddy viscosity, u_w is the modulus of the wave solution in the lower part of the wave boundary layer, U is the magnitude of the horizontal current, z is the vertical coordinate measured positive upwards from the bed and z_0 is the hydraulic roughness. Given profiles for the eddy viscosity, wave and current, the nonlinear system (2), (3) and (4) can be solved to produce the bottom stress vectors τ_{cw}, τ_{wm} and τ_c.

2.1 Small to intermediate roughness

For conditions in which the height of the roughness elements are small in comparison to the wave boundary layer thickness, Glenn (1983) proposed the following 3-layer continuous eddy viscosity over the original 2-layer discontinuous formulation used by GM:

$$\begin{aligned} K &= \kappa u_{*c} z & z &> z_2, \\ K &= \kappa u_{*cw} z_1 & z_1 &< z < z_2, \\ K &= \kappa u_{*cw} z & z_0 &< z < z_1, \end{aligned} \tag{5}$$

where κ is von Karman's constant (0.4), z_1 is an arbitrary constant scale height and $z_2 = z_1 u_{*cw}/u_{*c}$, which is determined by matching the eddy viscosities at $z = z_2$ (Figure 1a).

Substituting the above eddy viscosity into (3) gives

$$u_{*wm}^2 = \kappa u_{*cw} z_0 \frac{u_b}{l_{cw}} \Gamma_{ws}, \tag{6}$$

where the non-dimensional wave shear is defined by

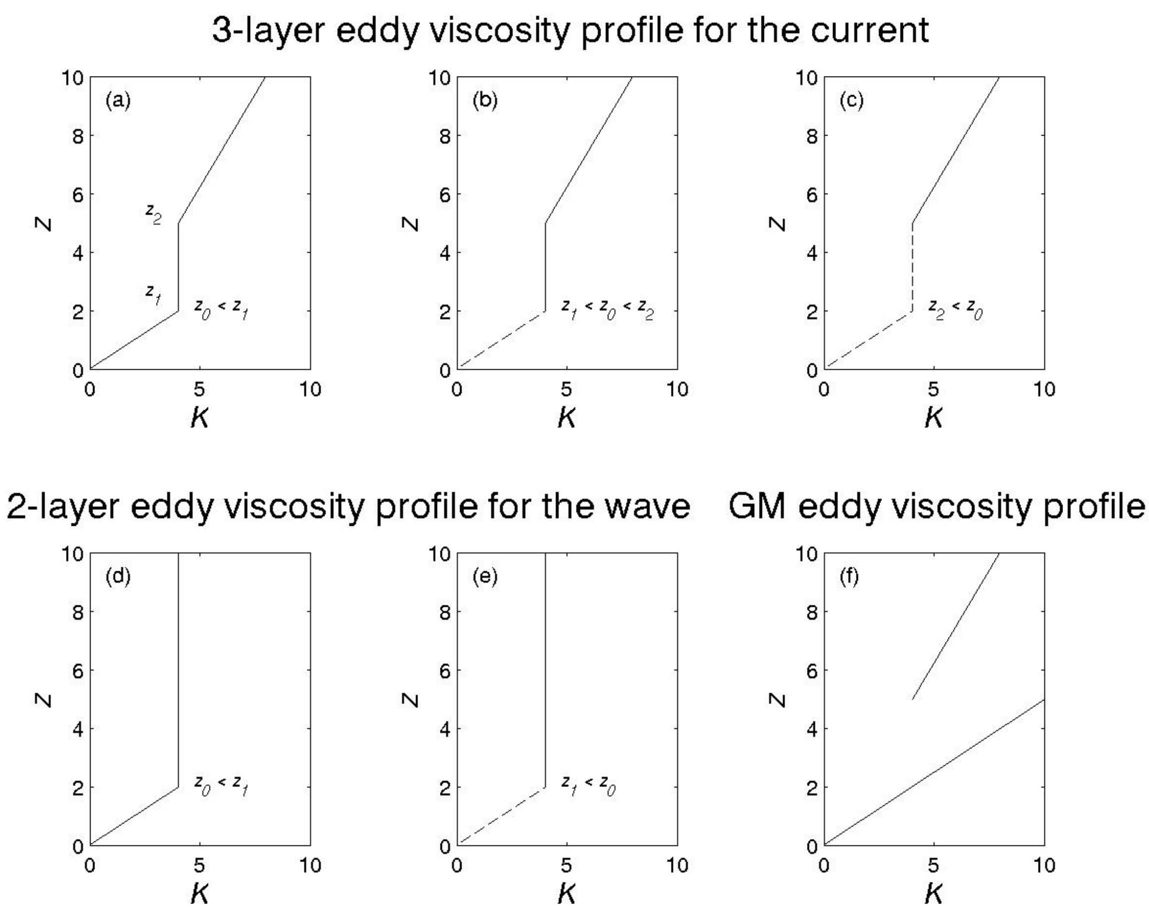

Figure 1 Schematic illustrating eddy viscosity profiles.

$$\Gamma_{ws} \equiv \frac{l_{cw}}{u_b} \frac{\partial u_w}{\partial z}\bigg|_{z = z_o} = \frac{1}{u_b} \frac{\partial u_w}{\partial \xi}\bigg|_{\xi = \xi_o}, \tag{7}$$

and u_b is the bottom wave orbital velocity. The non-dimensional vertical coordinate, $\xi = z/l_{cw}$ ($\xi_0 = z_0/l_{cw}$), is originally derived from GM's governing equation for the wave, where the scale height of the wave boundary layer for combined flows, l_{cw}, is defined by

$$l_{cw} = \kappa u_{*cw}/\omega \tag{8}$$

and ω is the wave radian frequency. Since several eddy viscosities will be explored in this analysis, the non-dimensional wave shear is introduced as a convenience. The solution to Γ_{ws} is provided in

Styles and Glenn (2000). By virtue of the eddy viscosity, (6) provides a relationship between u_{*wm} and u_{*cw}.

Substituting (5) into (4) and integrating gives the mean current profile:

$$
\begin{aligned}
U(z) &= \frac{u_{*c}}{\kappa} \ln\left(\frac{z}{z_2}\right) + U(z_2) && z_2 < z, \\
U(z) &= \frac{u_{*c}^2}{\kappa u_{*cw}} \frac{(z - z_1)}{z_1} + U(z_1) && z_1 < z < z_2, \\
U(z) &= \frac{u_{*c}^2}{\kappa u_{*cw}} \ln\left(\frac{z}{z_0}\right) && z_0 < z < z_1,
\end{aligned}
\quad \textbf{(9)}
$$

where the no-slip condition at z_0 and the matching requirement that the velocity be continuous at z_1 and z_2 have been imposed. Although (9) is an explicit solution for the current, in this application, a current, u_r, is specified at a given height off the bottom, z_r, and u_{*c} is calculated as an inverse problem. This produces a relationship between u_{*c} and u_{*cw}.

2.2 Large roughness

If the roughness length, k_b (= $30z_0$), and the wave boundary layer thickness are of the same order of magnitude, then the physical situation is indicative of a fully rough turbulent environment. Under these conditions, z_0 can become greater than z_1, and the no-slip condition is applied in the range $z_1 < z_0 < z_2$. The eddy viscosity is constant (Figure 1b) near the bed and the profile throughout the constant stress layer is given by

$$
\begin{aligned}
K &= \kappa u_{*c} z && z_2 < z, \\
K &= \kappa u_{*cw} z_1 && z_1 < z_0 < z < z_2.
\end{aligned}
\quad \textbf{(10)}
$$

The corresponding kinematic maximum wave stress becomes

$$
u_{*wm}^2 = \kappa u_{*cw} z_1 \frac{u_b}{l_{cw}} \Gamma_{ws}, \quad \textbf{(11)}
$$

where it is understood that Γ_{ws} implicitly reflects the change in the solution for the wave shear due to the fact that the eddy viscosity where the no-slip condition is applied is now constant instead of linearly increasing as in (5). The solution for Γ_{ws} is presented in Appendix A. Similarly, the solution for the current becomes

$$U(z) = \frac{u_{*c}}{\kappa} \ln\left(\frac{z}{z_2}\right) + U(z_2) \qquad z_2 < z,$$

$$U(z) = \frac{u_{*c}^2}{\kappa u_{*cw}} \frac{(z - z_0)}{z_1} \qquad z_1 < z_0 < z < z_2, \tag{12}$$

where the no-slip condition is now applied above z_1.

2.3 Large roughness with vanishingly small waves

For the case of vanishingly small waves, $z_2 \rightarrow z_1$ and z_0 may even become greater than z_2. The eddy viscosity where the no-slip condition is applied then becomes

$$K = \kappa u_{*c} z \qquad z_2 < z_0 < z \tag{13}$$

(Figure 1c), so that

$$u_{*wm}^2 = \kappa u_{*c} z_0 \frac{u_b}{l_{cw}} \Gamma_{ws}. \tag{14}$$

Note the change in velocity scale from u_{*cw} to u_{*c}, which is due to the eddy viscosity above z_2 being a function of u_{*c} and not u_{*cw}. This means that for very small, though finite waves, the much greater shear stress associated with the current can still affect the wave. The solution to Γ_{ws} for the eddy viscosity given by (13) is presented in Appendix A. Substituting (13) into (4), the current reduces to the classic logarithmic profile,

$$U(z) = \frac{u_{*c}}{\kappa} \ln\left(\frac{z}{z_0}\right) \qquad z_2 < z_0 < z. \tag{15}$$

2.4 Non-dimensionalization of the equations

An efficient solution algorithm can be obtained by recasting the bottom stress equations into a suitable non-dimensional form. Introducing u_{*cw} as the logical choice for the velocity scale produces the following non-dimensional parameters that will be useful in formulating the bottom stress solution:

$$\sigma = \frac{u_b}{u_{*cw}}, \qquad \epsilon = \frac{u_{*c}}{u_{*cw}}, \qquad \mu = \frac{u_{*wm}}{u_{*cw}}, \tag{16}$$

where σ is related to a combined wave and current friction factor ($\sigma = 1/\sqrt{f_{cw}/2}$), ϵ is a measure of the relative contribution from the current to the total stress, and μ is a measure of the relative contribution from the wave to the total stress. Squaring both sides of (2) and rearranging gives

$$u_{*c}^4 + 2\,u_{*wm}^2 \cos\phi_{cw}\, u_{*c}^2 + u_{*wm}^4 - u_{*cw}^4 = 0, \tag{17}$$

which is quadratic in u_{*c}^2 with the solution

$$u_{*c}^2 = -u_{*wm}^2 \cos\phi_{cw} + \sqrt{u_{*wm}^4(\cos^2\phi_{cw} - 1) + u_{*cw}^4}, \tag{18}$$

where the + is chosen to ensure that u_{*c} is positive. Dividing both sides of (18) by u_{*cw}^2 and substituting μ and ϵ from (16) yields

$$\begin{aligned} \epsilon^2 &= -\mu^2\cos\phi_{cw} + \sqrt{\mu^4(\cos^2\phi_{cw} - 1) + 1}, \\ &= -\mu^2\cos\phi_{cw} + \sqrt{1 - \mu^4\sin^2\phi_{cw}}. \end{aligned} \tag{19}$$

The kinematic stress for the wave has three different formulations corresponding to the expressions given by (6), (11) and (14). Dividing both sides of these equations by u_{*cw}^2 and substituting μ and σ from (16) gives

$$\begin{aligned} \mu^2 &= \kappa\,\xi_0\,\sigma\,\Gamma_{ws} && \xi_0 < \xi_1 < \xi_2, \\ \mu^2 &= \kappa\,\xi_1\,\sigma\,\Gamma_{ws} && \xi_1 < \xi_0 < \xi_2, \\ \mu^2 &= \kappa\,\xi_0\,\epsilon\,\sigma\,\Gamma_{ws} && \xi_2 < \xi_0. \end{aligned} \tag{20}$$

where $\xi_1 = z_1/l_{cw}$ and $\xi_2 = z_2/l_{cw}$. Similarly, (9), (12) and (15) can be used to formulate three separate expressions for σ. Rather than outlining the details for all three cases, the non-dimensionalization is illustrated using (9). Given a specified current, u_r, at a height, z_r, above z_2, and solving for σ yields

$$\sigma = \frac{\epsilon\, u_b}{\kappa\, u_r}\left[\ln\left(\frac{z_r}{z_2}\right) + 1 - \epsilon + \epsilon \ln\left(\frac{z_1}{z_0}\right)\right]. \tag{21}$$

If the observed current, u_r, is specified at values of z_r that are less than z_2 or z_1, but greater than z_0, three more equations emerge. The resulting solutions for all six formulations are listed in Table 1, along with their appropriate ranges of validity.

The results of the above derivations reveal that μ and σ are dependent on various non-dimensional length scales that arise from the eddy viscosity formulation and boundary conditions. These unspecified parameters still must be determined to obtain a closed solution. It can be shown that μ is a function of ξ_0, ξ_1, σ and ϵ. Only the first two remain unspecified and they will be addressed in turn.

The non-dimensional roughness height, ξ_0, can be written

$$\xi_0 = \frac{1}{\kappa R_*}, \tag{22}$$

where, in analogy with planetary boundary layers (e.g., Grant and Madsen 1986; Wiberg 1995), $R_* = u_{*cw}/z_0\omega$ is an internal friction Rossby number for combined flows. The parameter R_* can be interpreted as the ratio of the nonlinear interaction height to the flow roughness. According to Madsen and Wikramanayake (1991), the dimensional height z_1 is expected to be a function of the wave boundary layer thickness. Therefore, z_1 is written as, $z_1 = \alpha l_{cw}$, where α is a free parameter that represents the fraction of the wave boundary layer that the eddy viscosity varies linearly with height, and that must be determined experimentally. This defines $\xi_1 = \alpha$, which gives $\xi_2 = \alpha/\epsilon$. The parameter μ is now a function of R_*, α, σ and ϵ.

Examination of the various solutions presented in Table 1 shows that as a minimum

$$\sigma = \sigma\left(\frac{u_b}{u_r}, \frac{z_1}{z_0}, \frac{z_r}{z_1}, \epsilon, \alpha\right), \tag{23}$$

where the explicit functional dependance on z_2/z_1 and z_r/z_2 has been omitted as $z_2 = z_1/\epsilon$. Using the definition for l_{cw}, z_1/z_0 can be written $z_1/z_0 = \alpha\kappa R_*$. An analogous expression can be defined for z_1/z_r, i.e., $z_1/z_r = \alpha\kappa R_{*r}$, where $R_{*r} = u_{*cw}/(z_r\omega)$. The two expressions are related by $R_*/R_{*r} = z_r/z_0$, where z_r/z_0 is an independent external parameter. R_* and σ are also related since $R_*\sigma = u_b/\omega z_0 = A_b/z_0$. Equation (23) is now an implicit function of the external parameters u_b/u_r, z_r/z_0, A_b/z_0 and the internal

Table 1 Expressions for σ derived from the current solution discussed in the text. Inequalities signify applicable ranges for a given expression.

$\sigma = \frac{\epsilon u_b}{\kappa u_r}\left[\ln\left(\frac{z_r}{z_2}\right) + 1 - \epsilon + \epsilon \ln\left(\frac{z_1}{z_0}\right)\right]$ **(24)** $z_r > z_2 > z_1 > z_0$	$\sigma = \frac{\epsilon^2 u_b}{\kappa u_r}\left[\frac{z_r}{z_1} - 1 + \ln\left(\frac{z_1}{z_0}\right)\right]$ **(25)** $z_2 > z_r > z_1 > z_0$
$\sigma = \frac{\epsilon^2 u_b}{\kappa u_r}\ln\left(\frac{z_r}{z_0}\right)$ **(26)** $z_2 > z_1 > z_r > z_0$	$\sigma = \frac{\epsilon u_b}{\kappa u_r}\left[\ln\left(\frac{z_r}{z_2}\right) + \epsilon\left(\frac{z_2 - z_0}{z_1}\right)\right]$ **(27)** $z_r > z_2 > z_0 > z_1$
$\sigma = \frac{\epsilon^2 u_b}{\kappa u_r z_1}\left(z_r - z_0\right)$ **(28)** $z_2 > z_r > z_0 > z_1$	$\sigma = \frac{\epsilon u_b}{\kappa u_r}\ln\left(\frac{z_r}{z_0}\right)$ **(29)** $z_r > z_0 > z_2 > z_1$

parameters α and ϵ. It can be shown that ϵ is a function of A_b/z_0, σ, α and ϕ_{cw}, so that σ is a function of the external parameters u_b/u_r, z_r/z_0, A_b/z_0, ϕ_{cw} and the internal closure constant α. Although the system of coupled equations resulting from this analysis does not produce an algebraic expression for the shear stresses, a closed theoretical solution exists. The nonlinear system therefore can be solved iteratively.

2.5 Solution algorithm for the 3-layer model

The procedure adopted here is to recast the series of non-dimensional expressions derived above into a root finding algorithm for σ. Applying the pure current ($u_b = 0$) or pure wave ($u_{*cw} = u_{*wm}$) limit shows that σ is bounded by $0 \le \sigma \le u_b/u_{*wm}$. The solution for the pure wave limit is obtained by setting μ equal to 1 and can be computed independently of the combined stress solution. Depending on the root finding algorithm, at least one initial guess for σ is needed to start the iteration. For combined flows, we use the bisection method (Atkinson 1989) since the root is guaranteed to lie between the pure wave and pure current limits. The next step is to determine μ, which has a functional dependence that can be described by

$$\mu = \mu\left(\frac{A_b}{z_0}, \alpha, \sigma, \epsilon\right). \qquad \textbf{(30)}$$

The first two parameters are given, the third is assigned an initial value that lies between the universal limits and the last parameter is unknown. Recalling that ϵ is related to μ and the external parameter ϕ_{cw} through (19), an internally consistent value can be computed by recasting the coupled equations (19) and (20) into a root finding algorithm for ϵ similar to that used to determine σ. Again, the bisection method is chosen since ϵ is bounded by universal limits ($0 \leq \epsilon \leq 1$). Once μ and ϵ have been computed, z_1/z_0 is determined by $z_1/z_0 = \alpha\kappa R_* = \alpha\kappa A_b/z_0/\sigma$, and z_1/z_r is determined by $z_1/z_r = \alpha\kappa R_{*r} = \alpha\kappa A_b/z_r/\sigma$. The parameters z_2/z_r and z_2/z_0 are related to z_1/z_r and z_1/z_0 through ϵ, which is now known. Given the above estimates for these non-dimensional length scales, along with u_b/u_r, which is an external parameter, a new value for σ is computed from the equations listed in Table 1. The relative difference between the new and old value is checked to see if it is below some prescribed tolerance. If it is not, then the process is repeated until σ converges.

2.6 Simplification for μ

The solution procedure described above reveals that a nested iteration scheme is required, in which an inner loop is first initiated to produce internally consistent estimates of μ and ϵ, and then an outer loop is executed to solve for σ. These iterations represent the most computationally expensive operations in the stress solution. If the inner loop can be removed from the solution procedure, then the total number of computations will be reduced, increasing the speed of convergence.

Examination of the governing equation for the wave (Styles and Glenn 2000), indicates that the velocity scale (u_{*c}) for the stress term when $z > z_2$ is identical to the formulation above the wave boundary layer derived by GM. Using scaling arguments for the governing equation for the wave, GM demonstrated that as long as u_{*c} was on the order of the wave velocity or less, then the stress term for the wave outside the wave boundary layer could be neglected. For the case here, which considers pure currents as a possible limit, their assumption may not apply when the current is much stronger than the wave. Under these circumstances, the wave shear and associated wave stress for $z > z_2$ are relatively weak, so that the wave solution in the outer region is well described by the linear theory, except possibly under very rough conditions (Styles and Glenn 2000). If the stress term for the wave is neglected above z_2, then the solution for μ becomes independent of ϵ and therefore z_2. This eliminates the inner iteration loop required to produce an internally consistent value for μ and ϵ, and accelerates the speed of convergence without appreciably altering the results of the stress model based on a 3-layer eddy viscosity for μ.

Appendix B presents a derivation of Γ_{ws} and μ based on a simpler, continuous 2-layer eddy viscosity (Figure 1d,e), in which the stress term for the wave above z_2 is neglected. The solution procedure follows that described in Section 2.5 except that μ no longer depends on ϵ. Instead, ϵ is computed explicitly through (19).

3.0 Model results

To illustrate the properties of the stress model, results are presented based on the simplified solution for μ discussed in Section 2.6. The input parameters consist of the external variables A_b/z_0, z_r/z_0, u_b/u_r and ϕ_{cw}, and the internal closure constant α.

Because the stress model is designed for a broad range of input wave and current conditions that may be produced by a shelf circulation model, the parameter ranges for A_b/z_0 and z_r/z_0 are $10^{-3} \leq A_b/z_0 \leq 10^6$ and $1.01 \leq z_r/z_0 \leq 10^6$. The lower limit is chosen to represent a maximum relative roughness for the wave (z_0/A_b) of 10^3. The upper limit is chosen to represent a 100 cm current height (z_r) or excursion amplitude (A_b) over a ripple-free bed with a minimum grain diameter roughness of $\sim10^{-3}$ cm (10 μm). Other model parameters have been fixed with values of $\alpha = 1$, $\phi_{cw} = 0$ and u_b/u_r

= 1. The latter is chosen so that the wave and current outside the wave boundary layer are about the same order of magnitude. Past expressions for α have ranged between about 0.15 and 2 (Glenn 1983; Madsen and Wikramanayake 1991; Lynch et al. 1997). We therefore choose an intermediate value to illustrate the model characteristics.

3.1 Fundamental model characteristics

Figure 2 depicts selected internal model parameters identified in the text as a function of the independent external parameters z_r/z_0 and A_b/z_0. Individual model parameters show varying degrees of sensitivity to z_r/z_0 and A_b/z_0, especially for extreme values. The first two parameters, $\mu = u_{*wm}/u_{*cw}$ and $\epsilon = u_{*c}/u_{*cw}$, illustrate the dynamic features of the stress model since they define the relative proportions of the wave and current shear velocities to the total. The pure wave or pure current limits are easily interpreted graphically, as $\mu \rightarrow 1$ and $\epsilon \rightarrow 0$ for pure waves, and $\mu \rightarrow 0$ and $\epsilon \rightarrow 1$ for pure currents. As $z_r/z_0 \rightarrow 1$ for a fixed u_r, the current shear becomes very large. This results in a large stress associated with the current ($\epsilon \rightarrow 1$) that will dominate over the wave in the combined flow. As this ratio increases, the current shear begins to decrease, with an associated reduction in ϵ. Eventually, z_r/z_0 will become so large that the turbulent stresses associated with the current (for constant u_r) must vanish and $\epsilon = 0$. In this limit, the solution becomes that of a pure wave ($\mu \rightarrow 1$). The rate at which the pure wave limit is approached is also a function of A_b/z_0. For constant u_b, decreases in A_b/z_0 lead to greater frictional drag for the wave and an associated increase in bottom stress. This behavior is apparent in the first two plots, as the pure wave limit proceeds more rapidly as a function of z_r/z_0 for smaller A_b/z_0.

Another notable feature is that both μ and ϵ become independent of A_b/z_0 when this ratio is less than 1. This can be understood by examining the non-dimensional length scales z_1/z_0 and z_2/z_0 and the parameter σ as a function of z_r/z_0, when $10^{-3} \leq A_b/z_0 \leq 10^{-1}$. Figure 2 reveals that z_1/z_0 and z_2/z_0 are always less than 1 in this range, so that the eddy viscosity where the no-slip condition is applied becomes constant and $\mu^2 = \kappa \sqrt{\xi_1}\, \sigma$ (Appendix B). Substituting σ from (29) into the above expression for μ gives

$$\mu^2 = \sqrt{\xi_1}\, \epsilon \frac{u_b}{u_r} \ln\left(\frac{z_r}{z_0}\right) \qquad z_r > z_0 > z_2 > z_1, \tag{31}$$

which is independent of A_b/z_0. The parameter ϵ is related to μ through (19), so it too is independent of A_b/z_0.

The second group of parameters, z_1/z_0, z_2/z_0, z_1/z_r and z_2/z_r, represents the length scales of the flow. All four parameters exhibit a strong dependence on A_b/z_0, but only z_1/z_r and z_2/z_r are dependent on z_r/z_0 when this ratio becomes very large. An important consideration for modeling applications is that all four parameters are well behaved for the broad range of A_b/z_0 and z_r/z_0 used here. The only exception is when $z_r/z_0 = 1$ ($u_r = 0$), which is a degenerate case.

Γ_{ws} is sensitive to smaller values of z_r/z_0, and to A_b/z_0 as long as $z_1/z_0 > 1$. When $z_1/z_0 < 1$, the eddy viscosity that defines the maximum wave shear is constant, and the resulting equation for Γ_{ws}, which is derived in Appendix B, is independent of A_b/z_0. The final two parameters, R_* and σ,

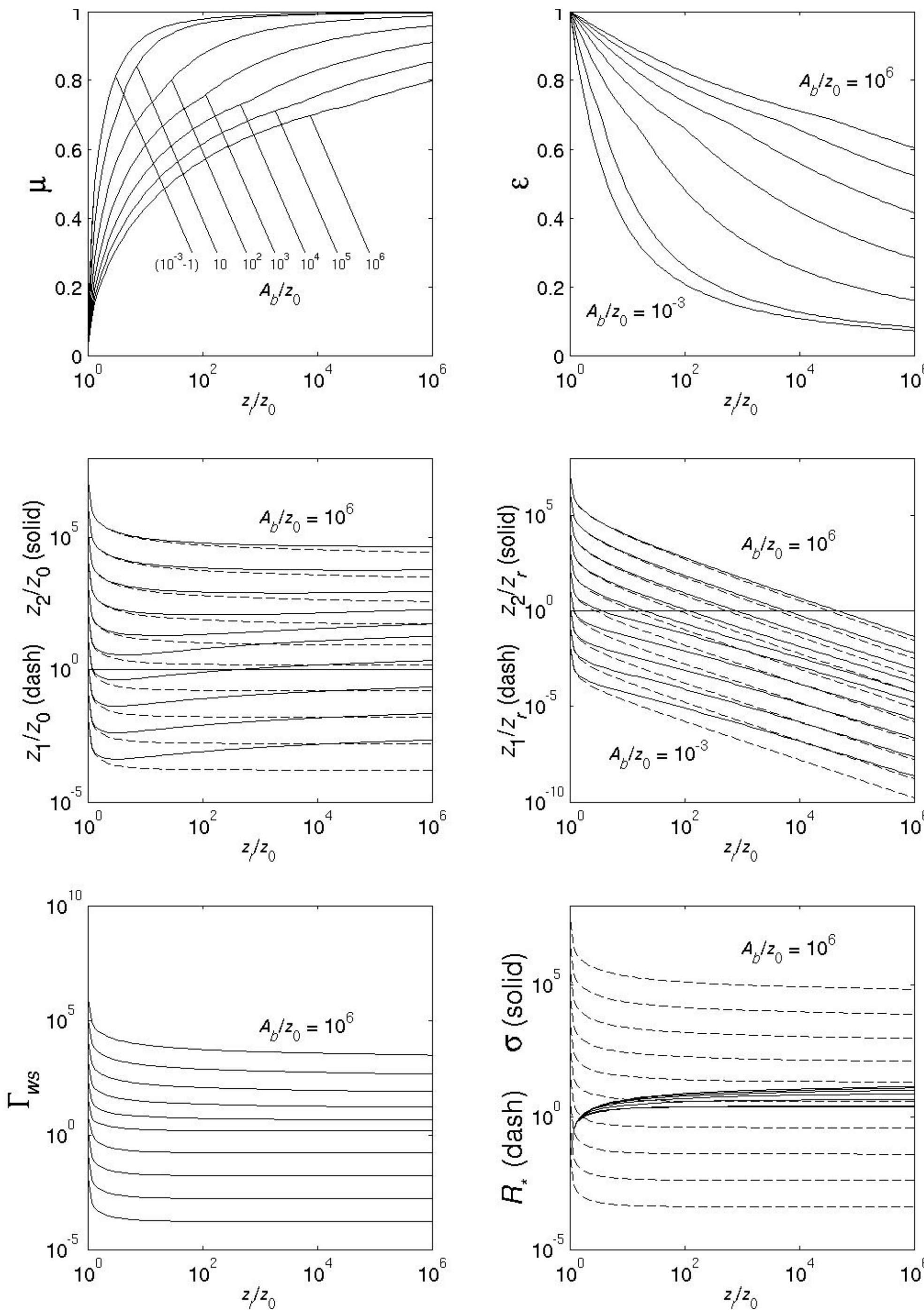

Figure 2 Selected internal model parameters as a function of z_r/z_0 and A_b/z_0. Definitions of the internal variables are provided in the text. Values for A_b/z_0 range from 10^{-3} to 10^6 in decadal increments.

are both sensitive to smaller values of z_r/z_0, and R_* is sensitive to A_b/z_0 for all values. The parameter σ is not very sensitive to the very large changes in either z_r/z_0 or A_b/z_0. This demonstrates the advantage of selecting σ as the function best suited for a root finding algorithm to close the stress solution.

The stress model also depends on u_b/u_r, which is a measure of the relative strength of the wave to the current. Figure 3 shows μ, ϵ and σ for the same conditions illustrated in Figure 2 but with $u_b/u_r = 10$ (large wave) and 0.1 (small wave). The general trends are the same as the $u_b/u_r = 1$ case, with the exception that for larger u_b/u_r, the solution approaches that of a pure wave much faster as a function of z_r/z_0, and for $u_b/u_r = 0.1$ the change is more gradual. Since a larger u_b/u_r signifies a stronger ambient wave, it is expected that the solution should converge to the pure wave limit much more rapidly as z_r/z_0 increases. The opposite is true for a relatively large current ($u_b/u_r = 0.1$). The parameter σ also is not as sensitive to A_b/z_0 when the current is much stronger than the wave.

3.2 Sensitivity to the direction between the wave and current

Equation (19) expresses a closed relationship between ϵ and μ given the external parameter ϕ_{cw}. A plot of ϵ as a function of μ for several values of ϕ_{cw} is shown in Figure 4. For small μ, ϵ is not very sensitive to μ or ϕ_{cw}. As μ becomes larger, and the shear stress associated with the wave becomes significant, ϵ becomes much more sensitive to ϕ_{cw}. This sensitivity can be described mathematically, since (19) reduces to

$$\epsilon^2 = 1 - \mu^2 \qquad \textbf{(32)}$$

for codirectional flow ($\phi_{cw} = 0$), and to

$$\epsilon^2 = \sqrt{1 - \mu^4} \qquad \textbf{(33)}$$

for orthogonal flow ($\phi_{cw} = \pi/2$). Both the larger exponent for μ and the radical in (33) tend to make ϵ larger when the wave and current are at right angles. Physically, this means that for a fixed maximum wave stress vector in the presence of a current, the magnitude of the time averaged shear stress must continually increase as ϕ_{cw} goes from 0 to $\pi/2$, if the magnitude of the maximum total stress vector is to remain constant. The direction of the maximum total stress vector will of course change as the time averaged shear stress vector rotates toward $\pi/2$. During storms, the wave and current vectors near the coast are generally at a high angle and both are relatively strong. If topographic steering or an evolving current (e.g., tides) produces local regions where ϕ_{cw} becomes small, an associated increase in the magnitude of the total shear stress may occur. There has been little observational work to characterize the stress field within the wave boundary layer for arbitrary wave and current vectors. Some preliminary studies seem to indicate that a first order effect is a reduction in the bottom roughness for the current as ϕ_{cw} increases (Sorenson et al. 1995; Styles 1998). This is due to ripples.

3.3 Bottom stress sensitivity to the eddy viscosity profile

The solution presented above neglects the stress term in the governing equation for the wave above z_2 but retains it for the current. This was justified on the assumption that u_{*c} was on the order of the wave velocity or less (GM). Styles and Glenn (2000) also have argued that the details of the eddy viscosity outside the wave boundary layer are not important in determining the bed stress

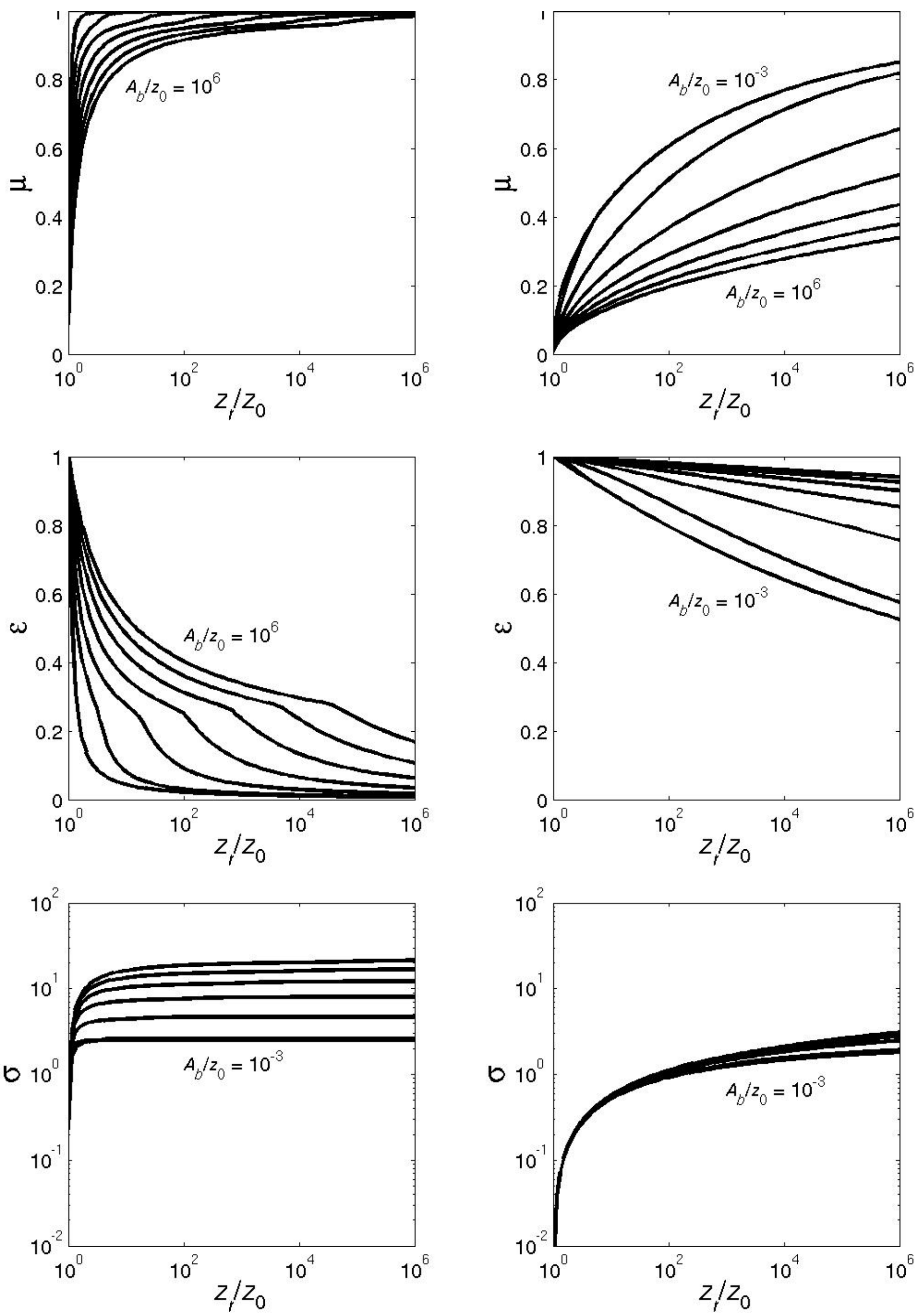

Figure 3 Similar to Figure 2, but showing only μ, ϵ and σ. Left column is for $u_b/u_r = 10$ (large waves) and right column is for $u_b/u_r = 0.1$ (large currents).

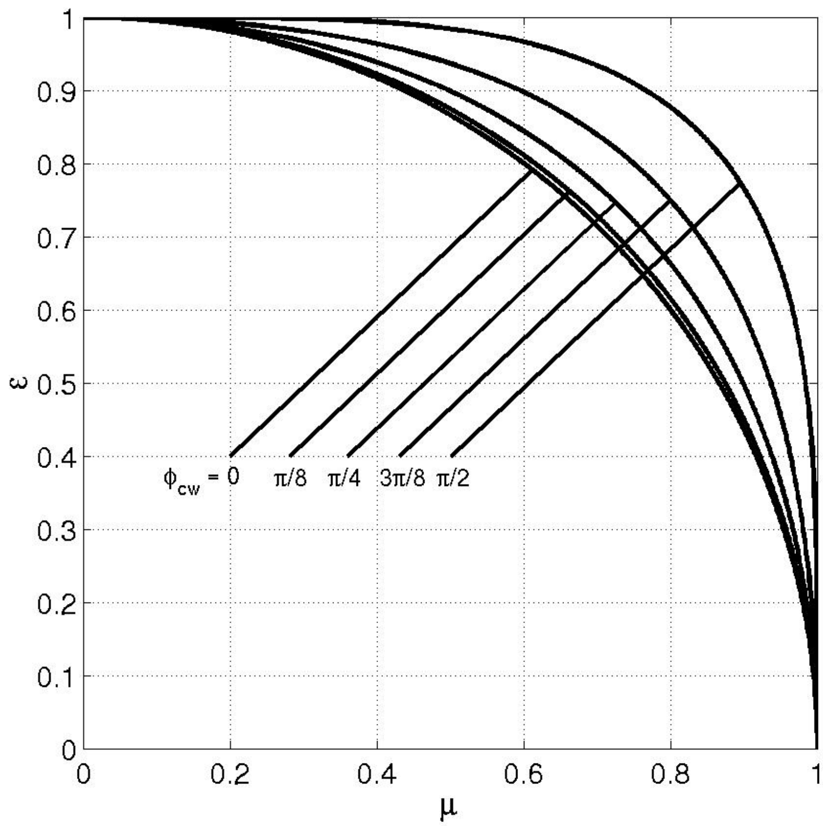

Figure 4 Sensitivity of the parameters ϵ and μ to the direction between the wave and the current.

except possibly for very rough beds. Both the Styles and Glenn (2000) 3-layer eddy viscosity depicted in Figure 1(a, b, c) and the simplified 2-layer continuous eddy viscosity for the wave depicted in Figure 1(d, e) are identical as $z \rightarrow z_0$, but diverge above z_2. Another eddy viscosity profile that has been used extensively in the past is the linearly increasing, discontinuous form originally proposed by GM (Figure 1f). Since all three formulations are different above the wave boundary layer but the same below z_1, the present stress model can be used to examine how the details of the eddy viscosity profile outside the wave boundary layer affect bed stress estimates.

A stress model based on the GM eddy viscosity does not include the z_1 or z_2 terms. Instead, GM prescribe the height of the wave boundary layer, δ_{cw}, which is also formulated as a constant, n, times l_{cw} ($\delta_{cw} = nl_{cw}$). For this comparison n is set equal to 2, which is the typical value used in applications (Glenn and Grant 1987; Madsen et al. 1993; Madsen 1994; Keen and Glenn 1994). To highlight the differences between the three eddy viscosity formulations, the ranges of the input variables are reduced to $10^{-1} \leq A_b/z_0 \leq 10^3$ and $1.01 \leq z_r/z_0 \leq 10^3$. Other parameters are set with values of $\phi_{cw} = 0$, $u_b/u_r = 1$ and $\alpha = 1$. To illustrate the dynamical properties of the three modeling approaches, the comparison focuses on the parameters μ, ϵ and σ, which are depicted in Figure 5. For $A_b/z_0 \geq 100$, all three models produce about the same result, and, therefore, the solution is not sensitive to the form of the eddy viscosity in the outer wave boundary layer and above. This point is argued by Styles and Glenn (2000), who claim that the stratification correction also introduces arbitrary changes to the eddy viscosity and, therefore, can be neglected in the wave stress solution.

For a larger relative roughness, the three solutions begin to diverge. This is most apparent for the 2-layer continuous eddy viscosity, which was shown to produce an upper bound on μ and a lower bound on ϵ and σ when $z_1/z_0 < 1$. The GM and Styles and Glenn (2000) eddy viscosity profiles for the wave are not constant in the outer portion of the constant stress layer, so that σ, μ and ϵ remain functions of A_b/z_0 when the relative roughness is very large.

In the limit of a pure current ($z_r/z_0 \rightarrow 1$), both μ and ϵ based on the stress models derived using the GM and Styles and Glenn (2000) eddy viscosities converge. This limit was mentioned above as a possible case when u_{*c} might be important in the governing equation for the wave outside the wave boundary layer. Since the result based on the Styles and Glenn (2000) eddy viscosity profile includes the stress term above z_2 and the GM eddy viscosity does not, the importance of retaining the stress term for this case appears minimal. The fact that the three models produce dissimilar results for a large relative roughness ($A_b/z_0 \lesssim 10$) suggests that careful consideration of the parameterization of the turbulent stresses for a rough bed is important.

3.4 Evaluation of α

The above analysis has revealed that the model is most sensitive to the eddy viscosity profile for very rough beds ($k_b/A_b \gtrsim 1.0$). On storm-dominated sandy continental shelves the roughest beds are speculated to be associated with the presence of relic ripples, which can have maximum ripple heights that exceed 10 cm (Traykovski et al. 1999). The amount of time that relic ripples dominate the roughness signature on sandy continental shelves is very hard to quantify considering the difficulties of obtaining long-term measurements of ripple degradation in the wake of storms. Assuming that relic ripples persist for some time after storm events, it is possible to estimate the average amount of time that relic ripples may be present. Studies of storm forced transport on the New Jersey shelf (Styles 1998) have indicated that the average storm, as defined by the time that the shear stress based on skin friction exceeds the minimum for the initiation of sediment motion, lasts about 24 hours and that approximately 10 such storms occur annually. Assuming that biological activity sufficiently degrades ripples within a week or two after a storm (Traykovski et al. 1999), gives an annual maximum relic ripple period of 2 to 5 months. This can be a significant amount of time and suggests that BBLMs must be properly calibrated for use in very rough conditions that are likely to occur on wave-dominated continental shelves.

Model sensitivity to the form of the eddy viscosity profile can be investigated by modulating the parameter α. If α is very large then the eddy viscosity in the vicinity of z_0 increases linearly. This is the same as the GM model deep within the wave boundary layer. For intermediate values of α, the eddy viscosity profile is identical to Madsen and Wikramanayake (1991) and Styles and Glenn (2000). If α is very small, then the eddy viscosity in the vicinity of z_0 is a constant, and it is similar to vertically independent forms that have been suggested for very rough beds (Nielsen 1992;Sleath 1991). Modifying α in the present model effectively reproduces the eddy viscosity profiles discussed above, which were shown to produce different results when k_b/A_b was greater than about 1.

For a given set of external wave, current and roughness conditions, the boundary shear stress becomes sensitive only to the value of α. In laboratory flumes, all of these parameters can easily be prescribed or measured independently of a combined flow model with the exception of the bottom roughness. This is because the precise mathematical formulation depends on the size and shape of the bedforms present, which means that k_b varies as a function of the experimental

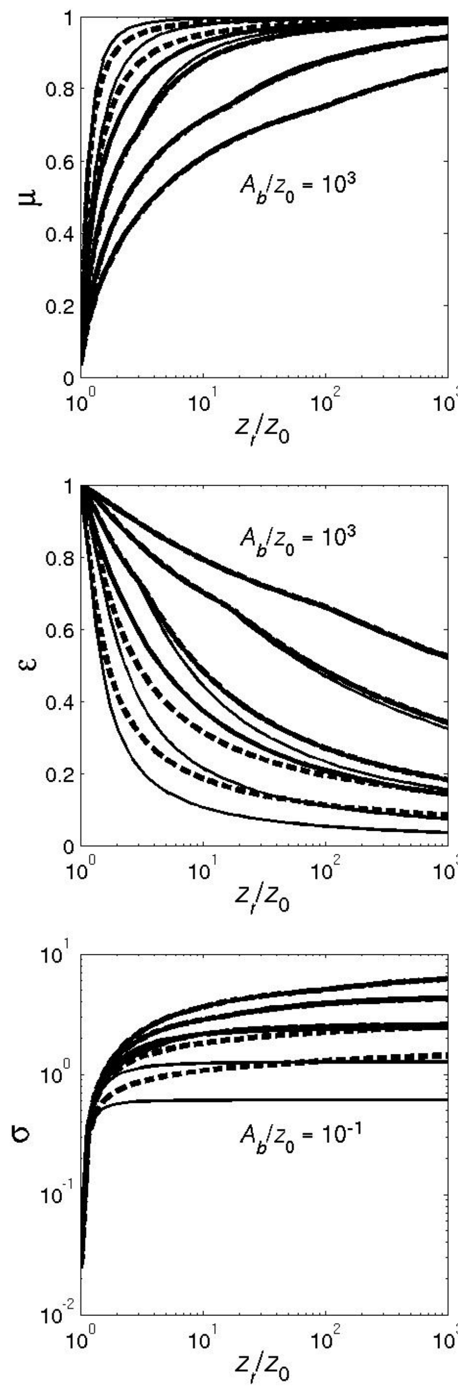

Figure 5 Comparison of μ, ϵ and σ for the GM (thin solid), Styles and Glenn (2000) (dash) and 2-layer continuous (thick solid) eddy viscosity profiles. A_b/z_0 ranges from 10^{-1} to 10^3 in decadal increments.

conditions and is not universal in form. Therefore, the experimental setting must conform as closely as possible to the actual environmental conditions to which the calibration results apply. In this case, the experimental conditions must include roughness elements that simulate the approximate shape of wave-generated ripples and more importantly they must return a consistent roughness value based on several independent methods of determination.

The data sets used to evaluate α for combined flows are obtained from Mathisen and Madsen (1995a, b) (hereinafter referred to as MM). MM conducted detailed experiments of co-directional wave and current flows in a laboratory flume. To ensure rough turbulent conditions, they modified the bed of their flume with triangular shaped bars that were scaled to simulate the geometry of 2-D wave-generated ripples. In nearly all of their experiments, $k_b/A_b > 1$, which is ideal for evaluating the present stress model for rough conditions. MM reported all necessary input data to drive the model including bottom roughness height and the wave friction factor, which was determined by measuring the decay in wave height over the length of the flume and relating that to dissipation due to bottom friction. Noting that $\mu/\sigma = \sqrt{f_w/2}$, friction factor curves can be generated and compared to their measurements. Setting k_b equal to the roughness determined for pure currents (MMa, Table 2) and using the measured water particle amplitudes, orbital velocities and mean currents, a family of friction factor curves as a function of α are generated. The current roughness is chosen since MM's results demonstrated that k_b was nearly the same for waves in the presence and absence of currents, and currents in the presence and absence of waves. Also, their current roughness estimates are independent of the GM combined wave and current model, whereas this model is used to determine the roughness for all their cases with waves. As noted above, increasing α leads to an eddy viscosity profile that is very similar to the GM formulation. The choice then to use the roughness for pure currents ensures that the present method to determine α is not inherently dependent on the GM model (through the bottom roughness), which may bias the results to favor larger values of α. To quantify the comparison between the model and data, we adopt the relative error defined by

$$\ln(e) = \left[\frac{1}{N}\sum_{i=1}^{N}\left(\ln(Y_i) - \ln(\overline{Y}_i)\right)^2\right]^{\frac{1}{2}}, \tag{34}$$

where Y_i is the measured data point, $\overline{Y}_i$ is the corresponding model estimate and N is the number of data points (Wikramanayake and Madsen 1991). The friction factor curve that minimizes e identifies the optimum α.

Using values that range from 0.15 to 2 (Glenn 1983; Madsen and Wikramanayake 1991; Lynch et al. 1997; Styles 1998), the lowest error (e = 1.3) is obtained when α is set equal to 0.75. The corresponding modeled wave boundary layer thickness, as determined by $\delta_{cw} = nl_{cw}$ (n = 2) is a factor of 3 too low when compared to the observed height derived from wave and current profile measurements in the flume. MM also underestimate the height of the wave boundary layer using the GM model. MM attribute the enhanced boundary layer thickness to the increased bed roughness associated with their fixed artificial roughness elements. Relic ripples may play a role similar to artificial roughness elements, and, therefore, may produce an enhanced boundary layer thickness relative to smoother flow conditions. Although the main purpose here is to describe an algorithm to compute the total bed stress, the resulting wave and current stress components are integral components of suspended sediment concentration and velocity profile models (i.e., Smith 1977;

Wiberg and Smith 1983; GM; Glenn and Grant 1987). A model designed to predict current and suspended sediment concentration profiles should be able to reproduce accurately both the friction factor (stress) and the wave boundary layer thickness.

The fact that the model tends to underestimate the thickness of the wave boundary layer, yet accurately predicts the wave friction factor, suggests that it is the internal length scales, which define the height and thickness of the various regions in the boundary layer, as opposed to the velocity scales, which define the shear stresses, that should be reexamined. The present and GM models have as adjustable internal length scales z_1 and δ_{cw}, respectively. We hypothesize that for very rough conditions ($k_b/A_b \gtrsim 1$) the constants multiplying l_{cw} in the definition of z_1 and δ_{cw} are now functions of the relative roughness. A very simple approximation that incorporates explicitly the relative roughness in the definition of z_1, but reverts to the existing formulation in the limit $k_b/A_b \rightarrow 0$ is to modify z_1 as $z_1 = \alpha\, l_{cw}(a_0 + a_1 k_b/A_b + a_2(k_b/A_b)^2 + ...)$. Since k_b/A_b is expected to become a leading order term only for very rough beds, the series can be truncated to first order to give, $z_1 = \alpha\, l_{cw}(1 + \beta k_b/A_b)$. A similar expression is proposed for δ_{cw}: $\delta_{cw} = n\, l_{cw}(1 + \beta k_b/A_b)$. For smooth to moderately rough turbulent conditions ($k_b/A_b \lesssim 0.1$) the GM model has been shown to accurately predict the shear stress and apparent roughness with $n = 2$ (e.g., Grant et al. 1984; Drake and Cacchione 1992; Drake et al. 1992). This leaves two undetermined parameters (α and β) that must be calibrated from data. Optimal values are found by choosing the combination that minimizes the relative difference for both the friction factor and the wave boundary layer thickness. Using a range of values for β similar to those chosen for α, the lowest error ($e = 1.2$) is obtained when $\alpha = 0.3$ and $\beta = 0.7$. The results for combined flows are presented in Figure 6. The model compares well with the measured combined wave and current friction factors, and the average wave boundary layer thickness of 6.2 cm determined from the model ($\alpha = 0.3$) compares well with the measured value of 6 cm.

MM also conducted experiments for pure waves (MMa, Table 1). The roughness elements were the same as in the combined flow and pure current cases. Given that MM demonstrated similar roughnesses for waves in the presence and absence of currents permits an additional opportunity to refine the closure parameters in the case of pure waves. Setting the roughness height equal to the average obtained by MM for the pure current case, and using their experimental input wave parameters, friction factor curves are generated from the model and compared to their data. The results are shown in Figure 7. The lowest error ($e = 1.2$) for the friction factor was obtained with $\alpha = 0.3$ and $\beta = 0.8$. The average wave boundary layer thickness determined from the model was 6.0 cm. When β was set equal to 0.7 the lowest error for the friction factor still occurred with $\alpha = 0.3$, but the modeled wave boundary layer thickness had a mean of 5.4 cm. In both the combined and pure wave case, a consistent result emerges in which the calibration coefficients maintain similar values. It must be emphasized that the suggested values for the closure constants are only valid as long as they are applied to the stress model presented above (MM). Other wave/current bottom boundary layer models that include similar modifications must be calibrated before they should be used in applications.

The modifications presented above are not without a theoretical or empirical basis. The first order correction to z_1 leads to an eddy viscosity profile that is similar in functional form to expressions developed by Nielsen (1992) and Sleath (1991). For rough oscillatory flow very near the bed, Nielsen (1992) proposed the eddy viscosity $K = 0.004 A_b^{3/2} k_b^{1/2} \omega$ for $A_b/k_b < 16$. Similarly, Sleath (1991) suggested $K = 0.0025 A_b k_b \omega$ in the range $1 < A_b/k_b < 120$. Both expressions share a common functional dependence, namely the nonlinear product $A_b^c k_b^d \omega$, with the constraint that $c + d = 2$. The calibration results presented above are formulated in terms of an eddy viscosity in the

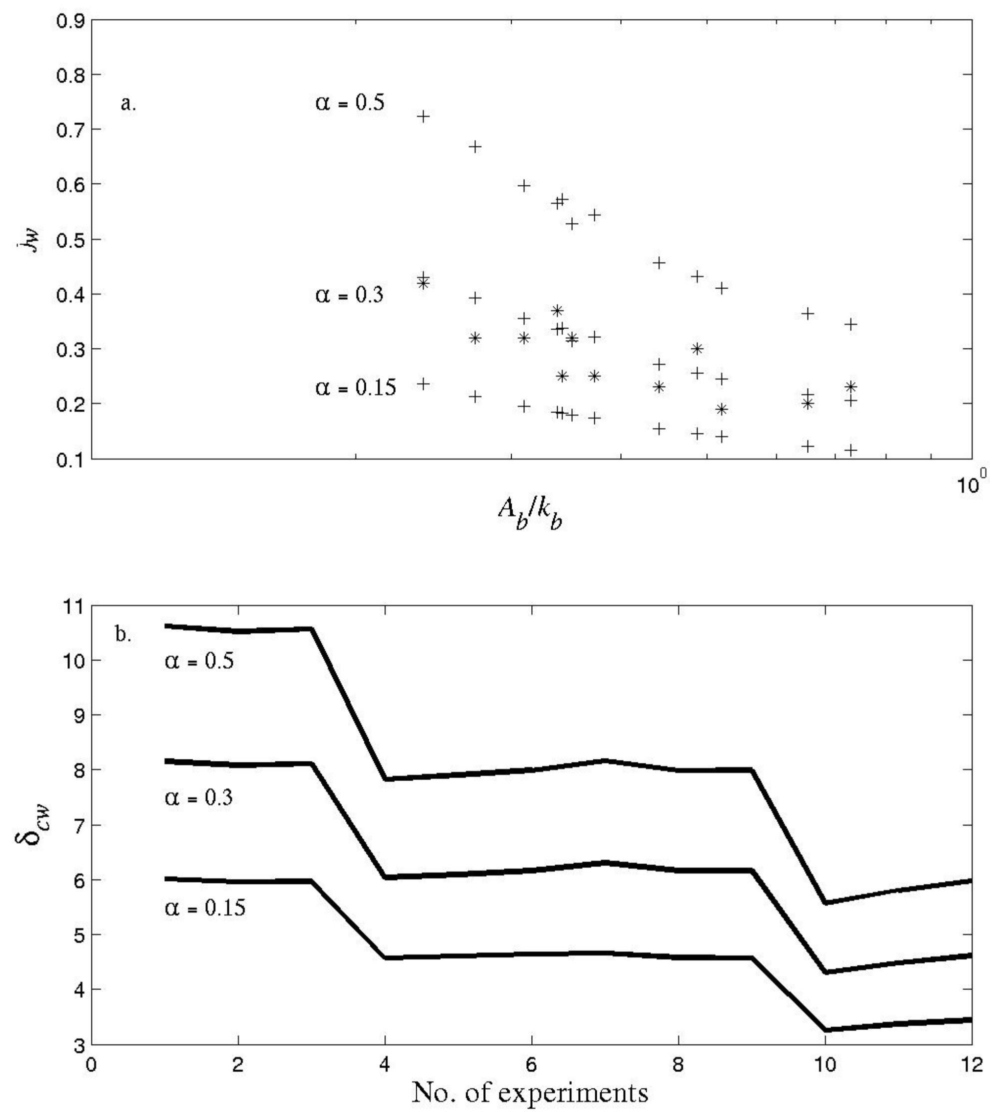

Figure 6 Combined wave and current model calibration results for the closure parameters α and β. (a) Measured (*) and modeled (+) friction factors as a function of α, including the best fit (α = 0.3). (b) Modeled wave boundary layer thickness for each of the 12 combined flow experiments carried out by MM as a function of α. Note that the family of friction factor curves are not smooth, since f_w for combined flows is a function of A_b/k_b, α and ϵ (Styles and Glenn 2000).

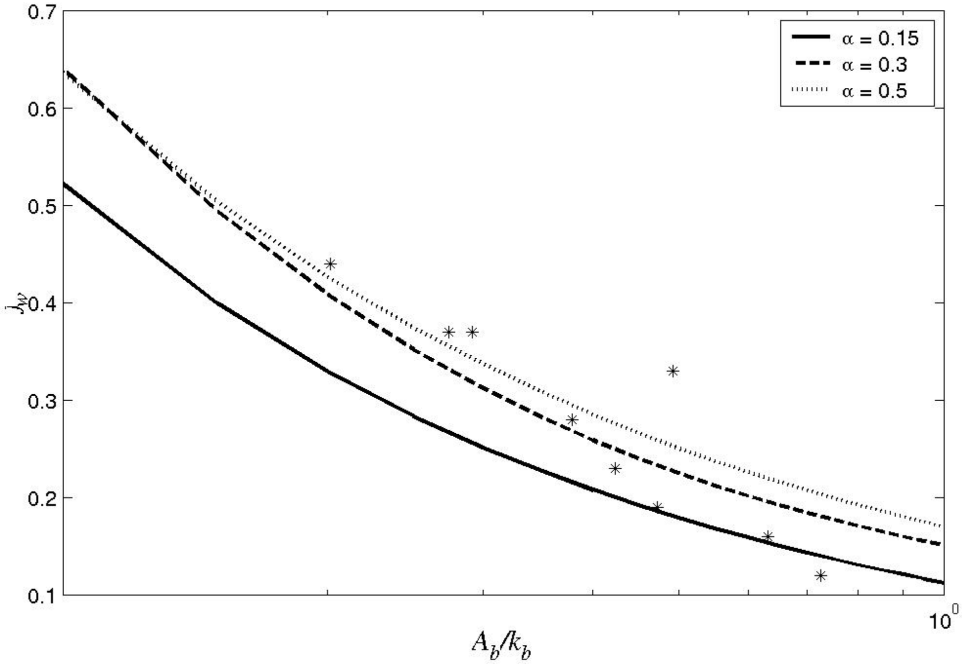

Figure 7 Pure wave model calibration results for the closure parameters α and β.

transition layer ($z_1 < z < z_2$) that is written as $K = \kappa\, u_{*cw}\, z_1$, with $z_1 = \alpha\, l_{cw}(1 + \beta k_b/A_b)$. Like the Nielsen (1992) and Sleath (1991) results, this modification leads to an eddy viscosity profile that is also an implicit nonlinear function of the product $A_b k_b \omega$. To illustrate, we consider a pure wave in which the roughness is large enough so that $z_1/z_0 < 1$. In this case the eddy viscosity becomes $K = \kappa\, u_{*wm} \alpha l_{wm}(1 + \beta k_b/A_b)$. Noting that $u_{*wm}/u_b = \sqrt{f_w/2}$ along with the definition of l_{wm} ($= \kappa u_{*wm}/\omega$), the eddy viscosity can be written as $K = \alpha\kappa^2 f_w/2A_b\omega(A_b + \beta k_b)$. Expanding this expression, say, for constant f_w, gives an eddy viscosity that is proportional to $A_b k_b\, \omega$, which has the same functional form as Sleath (1991). Depending of the definition of f_w, other nonlinear expressions emerge. As an example, Kajiura (1968) derived a friction factor of the form $f_w = 0.35(k_b/A_b)^{2/3}$. Substitution of this expression gives $K = 0.175\alpha\kappa^2(A_b^{4/3}k_b^{2/3}\omega + \beta A_b^{1/3}k_b^{5/3}\omega)$. Although this functional form is different from the results of Nielsen (1991) or Sleath (1992), all three formulations share a common nonlinear dependence on the same external parameters k_b, A_b and ω. The present modification, in that the explicit dependence on k_b/A_b vanishes in the limit of smoother bed conditions, is somewhat more general than the Nielsen (1992) and Sleath (1991) models that apply only for k_b/A_b greater than about 0.008.

3.5 Speed of convergence tests

An advantage of the solution algorithm described above is that the nested iteration scheme used in the Styles and Glenn (2000) and the family of Grant, Madsen and Glenn models (GM; Glenn and Grant 1987) can be avoided. Since the iterative root finding algorithm is the most computationally expensive step in the solution procedure, it is of great advantage if the number of times this operation must be executed can be substantially reduced. In fact, Keen and Glenn (1994) spent considerable effort to optimize the initial guess for the friction factor and other variables to speed the convergence in their streamlined version of the GM BBLM.

To illustrate the computational advantage of the present approach over the Styles and Glenn (2000) model, which uses the same eddy viscosity profile but still uses a nested iteration scheme, results of a speed of convergence test are presented. Because the Styles and Glenn (2000) model is restricted to a much narrower range of wave, current and roughness environments, the input parameters represent only a small subset of the full capabilities of the stress model presented here. The values of the input parameters, normalized run-time and total number of iterations are listed in Table 2. Each row represents 10,000 independent model runs with identical input and initial conditions. The run-time was recorded for each run, and normalized to produce the numbers listed in Table 2. The numbers in parentheses under the Styles and Glenn (2000) model denote the maximum number of iterations required to converge the friction factor. The other set of numbers denote the number of iterations required to converge u_{*c} in the Styles and Glenn (2000) model and σ in the present model. The Styles and Glenn (2000) model uses the secant method, while the present model uses a variation of Brent's root finding algorithm (Atkinson 1989), in which the iterations are performed using the bisection method but convergence is checked using the secant method after only a few iterations. A stopping tolerance of 10^{-4}, or a 0.01% relative error between the previous and present iteration is designated to established convergence. The results indicate that in all cases, convergence proceeds with fewer iterations, is at least twice as fast, and in some cases an order of magnitude faster, thus illustrating the greater efficiency of the bottom stress algorithm presented here. A similar speed of convergence comparison was performed between the present and the GM model, which can also be formulated without a nested iteration scheme (Grant and Madsen 1986). The results were similar except for the smoother conditions ($k_b = 1$ or 10), in which case the present formulation usually converged 20 to 30 percent faster. Since the present model uses a more physically reasonable eddy viscosity profile, has a correction to produce accurate estimates of the wave boundary layer thickness for very rough beds, and is more efficient for smoother conditions than the Grant and Madsen (1986) model, it is recommended for applications in which estimates of the near-bed flow and suspended sediment concentration profiles are desired.

4.0 Summary

We have presented a fairly robust algorithm to compute the enhanced wave and current boundary shear stress components for an unstratified bottom boundary layer. The stress model was designed for a broad range of wave and current flows, and was formulated without the need to introduce fictitious currents in the constant stress layer to obtain closure. Instead, the governing equations for the wave and current were reviewed and used to identify important velocity and length scales that could characterize the flow for a broad range of wave and current conditions, including the limiting case of pure waves or pure currents. Systematic non-dimensionalization of the governing equations revealed three important internal parameters: $\epsilon = u_{*c}/u_{*cw}$, $\mu = u_{*wm}/u_{*cw}$ and $\sigma = u_b/u_{*cw}$. It was demonstrated that interpreting the functional dependence of ϵ, μ and σ graphically helped to illustrate model stability and to distinguish the effects of different turbulence closure methods (i.e., different eddy viscosity formulations). The bed shear stress was most sensitive to the form of the eddy viscosity in the outer wave boundary layer and above for rough flow conditions

Table 2 Speed of convergence tests comparing the present method with the unstratified version of the Styles and Glenn (2000) wave and current BBLM. For all model runs, $\phi_{cw} = 0$ and $z_r = 100$ cm. The first three rows are for strong waves and currents (SS), the middle three rows are for strong waves and weak currents (SW), and the last three rows are for weak waves and strong currents (WS). The last two columns list normalized run-time (RT) and total number of iterations (N) for each method. The Styles and Glenn (2000) model uses a nested iteration scheme. The numbers in parentheses indicate the maximum number of iterations for the inner loop, which usually occurred during the first or second iteration of the outer loop.

	u_b (cm/s)	A_b (cm)	u_r (cm/s)	k_b (cm)	Present RT	Present N	Styles & Glenn RT	Styles & Glenn N
SS1	50	100	20	1.0	1	7	3.6	5 (10)
SS2	50	100	20	10	1	7	2.8	5 (9)
SS3	50	100	20	100	1	5	2.9	5 (7)
SW1	50	100	1	1.0	1	8	4.4	7 (8)
SW2	50	100	1	10	1	9	2.6	7 (7)
SW3	50	100	1	100	1	9	2	6 (6)
WS1	1	2	50	1.0	1	4	21	3 (37)
WS2	1	2	50	10	1	6	7.3	5 (17)
WS3	1	2	50	100	1	5	7	5 (18)

For very rough conditions, available combined wave and current data were utilized to refine estimates of the empirical constant α. In order to resolve the discrepancy between past formulations that produced accurate estimates of the friction factor but underestimated the thickness of the wave boundary layer, the scale heights z_1 and δ_{cw} were modified to include an explicit dependence on the relative roughness. This introduced and additional closure constant, β, that was determined experimentally to be about 0.7 for combined flows and 0.8 for pure waves. Further analysis of combined wave and current flows over very rough beds in natural flows is needed before a definitive value can be prescribed to model the constant stress portion of the bottom boundary layer. Until then, it is presently suggested that $\alpha = 0.3$ and $\beta = 0.7$ for applications of the stress model presented here.

Speed of convergence tests revealed that the present model converged in fewer total iterations and much faster than the Styles and Glenn (2000) BBLM, which used the same eddy viscosity profile. Faster convergence was attributed to the more efficient solution method, which avoided the nested iteration scheme used by Styles and Glenn (2000) and the family of Grant, Madsen and Glenn models.

Acknowledgments

Support for this research was provided through the National Oceanographic Partnership Program (NOPP) under grants N00014-97-1-1019 and N00014-98-1-0815, the Coastal Ocean Modeling and Observation Program (COMOP) under grant N00014-97-1-0797, the National Science Foundation under grant OCE-95-21102, and the Middle Atlantic Bight National Undersea Research Program under grant MAB 96-10 and NA06RU0139.

Appendix A

Here we present a derivation of Γ_{ws} and μ for the eddy viscosity in (5) when ξ_0 is greater than ξ_1 or ξ_2. Invoking the usual linear and boundary layer approximations, Styles and Glenn (2000) present the governing equation for the wave within the wave boundary layer for the 3-layer eddy viscosity as

$$\begin{aligned} iW - \frac{\partial}{\partial \xi}\xi\epsilon\frac{\partial W}{\partial \xi} &= 0 \qquad && \xi_2 < \xi, \\ iW - \frac{\partial}{\partial \xi}\xi_1\frac{\partial W}{\partial \xi} &= 0 && \xi_1 < \xi < \xi_2, \\ iW - \frac{\partial}{\partial \xi}\xi\frac{\partial W}{\partial \xi} &= 0 && \xi_0 < \xi < \xi_1, \end{aligned} \tag{35}$$

where $W = u_w - u_b$. We have assumed a simple harmonic motion ($e^{i\omega t}$) so that the time dependence is separable from the ξ dependence. With the appropriate boundary and matching conditions (Styles and Glenn 2000), the solution for the modulus of the wave is written

$$\begin{aligned} u_w &= |u_b + G(Ker\,2\sqrt{\xi/\epsilon} + iKei\,2\sqrt{\xi/\epsilon})| \qquad && \xi_2 < \xi, \\ u_w &= |u_b + Ce^{m\xi} + De^{-m\xi}| && \xi_1 < \xi < \xi_2, \\ u_w &= |u_b + A(Ber\,2\sqrt{\xi} + iBei\,2\sqrt{\xi}) \\ &\quad + B(Ker\,2\sqrt{\xi} + iKei\,2\sqrt{\xi})| && \xi_0 < \xi < \xi_1, \end{aligned} \tag{36}$$

where A, B, C, D and G are complex constants, Ber, Bei, Ker and Kei are zero order Kelvin functions and $m = \sqrt{i/\xi_1}$. For convenience, we have dispensed with the $e^{i\omega t}$ term since in this example the modulus of a complex number ($f + ig$) times $e^{i\omega t}$ is simply the modulus of $f + ig$. The values of the constants can be found in Madsen and Wikramanayake (1991) and reflect the specific condition that $\xi_0 < \xi_1 < \xi_2$. Based on the governing equation (35) and solution (36), it is possible to extend the wave solution to include cases when $\xi_1 < \xi_0 < \xi_2$ and $\xi_1 < \xi_2 < \xi_0$.

Case 1) $\xi_1 < \xi_0 < \xi_2$

Using the eddy viscosity profile given in (10), the governing equation for W can be written as

$$iW - \frac{\partial}{\partial\xi}\xi\epsilon\frac{\partial W}{\partial\xi} = 0 \qquad \xi_2 < \xi\,,$$

$$iW - \frac{\partial}{\partial\xi}\xi_1\frac{\partial W}{\partial\xi} = 0 \qquad \xi_0 < \xi < \xi_2\,. \tag{37}$$

Invoking the no-slip condition at the bed and given that the solution smoothly approaches the potential flow result at the top of the boundary layer, the corresponding solution for the wave modulus is

$$u_w = |u_b + G'(Ker\,2\sqrt{\xi/\epsilon} + iKei\,2\sqrt{\xi/\epsilon})| \qquad \xi_2 < \xi,$$

$$u_w = |u_b + C'e^{m\xi} + D'e^{-m\xi}| \qquad \xi_0 < \xi < \xi_2\,, \tag{38}$$

where,

$$C' = \frac{-u_b L}{P_0 L + M_0 N}\,, \qquad D' = \frac{-u_b N}{P_0 L + M_0 N} \tag{39}$$

and

$$G' = 2\left[\frac{C'P_2 + D'M_2}{K_2} + p\left(\frac{C'P_2 - D'M_2}{K_2^{(1)}}\right)\right]. \tag{40}$$

The terms in (39) and (40) are defined as follows:

$$M_0 = e^{-m\xi_0}, \qquad M_2 = e^{-m\xi_2},$$

$$P_0 = e^{m\xi_0}, \qquad P_2 = e^{m\xi_2},$$

$$K_2 = Ker\,2\sqrt{\xi_2/\epsilon} + i\,Kei\,2\sqrt{\xi_2/\epsilon}, \tag{41}$$

$$K_2^{(1)} = \frac{\partial}{\partial\xi}\left(Ker\,2\sqrt{\xi_2/\epsilon} + i\,Kei\,2\sqrt{\xi_2/\epsilon}\right)\Bigg|_{\xi = \xi_2},$$

$$L = M_2(mK_2 + K_2^{(1)}), \qquad N = P_2(mK_2 - K_2^{(1)}).$$

Substituting the wave solution into (7), Γ_{ws} becomes

$$\Gamma_{ws} = \left| m\left[\frac{M_0 N - P_0 L}{M_0 N + P_0 L}\right]\right| \tag{42}$$

and

$$\mu^2 = \kappa\,\xi_1\,\sigma\,\Gamma_{ws}. \tag{43}$$

Case 2) $\xi_1 < \xi_2 < \xi_0$

For this case (13) defines the eddy viscosity (Figure 1c), so that the solution for the wave modulus in the vicinity of ξ_0 becomes

$$u_w = u_b\left| 1 - \frac{Ker\,2\sqrt{\xi/\epsilon} + iKei\,2\sqrt{\xi/\epsilon}}{Ker\,2\sqrt{\xi_0/\epsilon} + iKei\,2\sqrt{\xi_0/\epsilon}}\right| \qquad \xi_2 < \xi_0. \tag{44}$$

Inserting (44) into (7) gives

$$\Gamma_{ws} = \left| \frac{-\dfrac{\partial}{\partial\xi}\left(Ker\,2\sqrt{\xi/\epsilon} + i\,Kei\,2\sqrt{\xi/\epsilon}\right)\Big|_{\xi = \xi_0}}{Ker\,2\sqrt{\xi_0/\epsilon} + i\,Kei\,2\sqrt{\xi_0/\epsilon}}\right| \tag{45}$$

and

$$\mu^2 = \kappa\,\xi_0\,\epsilon\,\sigma\,\Gamma_{ws}\,. \tag{46}$$

Appendix B

Here we present the solution for Γ_{ws} and μ while neglecting the stress term in the governing equation for the wave above ξ_2.

Case 1) 2-layer eddy viscosity ($z_0 < z_1$)

For the 2-layer eddy viscosity presented in Figure 1d, the governing equation for W is similar in form to the lower two layers in (35). Applying the appropriate boundary and matching conditions, the modulus of the wave solution becomes

$$\begin{aligned} u_w &= |u_b + D''e^{-m\xi}| && \xi_1 < \xi\,, \\ u_w &= |u_b + A'(Ber\,2\sqrt{\xi} + iBei\,2\sqrt{\xi}) \\ &\quad + B'(Ker\,2\sqrt{\xi} + iKei\,2\sqrt{\xi})| && \xi_0 < \xi < \xi_1\,, \end{aligned} \tag{47}$$

where

$$A' = \frac{-u_b N'}{B_0 N' - K_0 L'}\,, \qquad B' = \frac{-u_b L'}{K_0 L' - B_0 N'} \tag{48}$$

and

$$D'' = \frac{A'(B_1 + B_1^{(1)}) + B'(K_1 + K_1^{(1)})}{M_1(1 - m)}\,. \tag{49}$$

The terms in (48) and (49) are defined as follows:

$$K_0 = Ker\,2\sqrt{\xi_0} + i\,Kei\,2\sqrt{\xi_0}, \qquad B_0 = Ber\,2\sqrt{\xi_0} + i\,Bei\,2\sqrt{\xi_0},$$

$$K_1 = Ker\,2\sqrt{\xi_1} + i\,Kei\,2\sqrt{\xi_1}, \qquad B_1 = Ber\,2\sqrt{\xi_1} + i\,Bei\,2\sqrt{\xi_1},$$

$$K_1^{(1)} = \frac{\partial}{\partial \xi}\left(Ker\,2\sqrt{\xi_1} + i\,Kei\,2\sqrt{\xi_1}\right)\Bigg|_{\xi = \xi_1},$$

$$B_1^{(1)} = \frac{\partial}{\partial \xi}\left(Ber\,2\sqrt{\xi_1} + i\,Bei\,2\sqrt{\xi_1}\right)\Bigg|_{\xi = \xi_1}, \tag{50}$$

$$L' = m\,B_1 + B_1^{(1)}, \qquad N' = m\,K_1 + K_1^{(1)},$$

$$M_1 = e^{-m\,\xi_1}.$$

Substituting the modulus into (7) yields

$$\Gamma_{ws} = \left| -\left[\frac{N'B_0^{(1)}}{B_0 N' - K_0 L'} + \frac{L'K_0^{(1)}}{K_0 L' - B_0 N'}\right]\right|, \tag{51}$$

and

$$\mu^2 = \kappa\,\xi_0\,\sigma\,\Gamma_{ws}. \tag{52}$$

Case 2) 2-layer eddy viscosity ($z_0 > z_1$)

If ξ_0 is greater than ξ_1, the wave modulus becomes

$$u_w = \left| u_b\,[\,1 - e^{-m(\xi - \xi_0)}] \right| \qquad \xi_1 < \xi_0 < \xi. \tag{53}$$

With the aid of (7), Γ_{ws} takes on the simple form

$$\Gamma_{ws} = |\,m\,| \tag{54}$$

and

$$\mu^2 = \kappa\,\xi_1\,\sigma\,\Gamma_{ws} = \kappa\sqrt{\xi_1}\,\sigma. \tag{55}$$

References

Atkinson, K. E., 1989: *An introduction to numerical analysis*. John Wiley & Sons, Inc., 693 pp.

Cacchione, D. A. and Drake, D. E., 1982: Measurements of storm-generated bottom stresses on the continental shelf. J. Geophys. Res., 87, 1952-1960.

Cooper, C. and Thompson, J. D., 1989: Hurricane-generated currents on the outer continental shelf. 1: Model formulation and verification. J. Geophys. Res., 94, 12,513-12,539.

Davies, A. G. and Villaret, C., 1997: Oscillatory flow over rippled beds: Boundary layer structure and wave-induced Eulerian drift. Gravity Waves in Water of Finite Depth, M. Rahman, Ed., Computational Mechanics, 10, 215-254.

Davies, A. M. and Lawrence, J., 1993: Examining the influence of wind and wind wave turbulence on tidal currents, using a three-dimensional hydrodynamic model including wave-current interaction. J. Phys. Oceanogr., 24, 2441-2460.

Dingler, J. R., 1974: Wave-formed ripples in nearshore sands. Ph.D. thesis, Univ. of California, San Diego, 136 pp.

Drake, D. E. and D.A. Cacchione, 1992: Wave-current interaction in the bottom boundary layer during storm and non-storm conditions: observations and model predictions. Cont. Shelf Res., 12, 1331-1352.

Drake, D. E., Cacchione, D. A. and Grant, W. D., 1992: Shear stress and bed roughness estimates for combined wave and current flows over a rippled bed. J. Geophys. Res., 97, 2319-2326.

Glenn, S. M., 1983: A continental shelf bottom boundary layer model: The effects of waves, currents, and a movable bed. Sc.D. thesis, Mass. Inst. of Technol., Cambridge, 141 pp.

Glenn, S. M. and Grant, W. D., 1987: A suspended sediment correction for combined wave and current flows. J. Geophys. Res., 92, 8244-8246.

Grant, W. D. and Madsen, O. S., 1979: Combined wave and current interaction with a rough bottom. J. Geophys. Res., 89, 1797-1808.

Grant, W. D. and Madsen, O. S., 1986: The continental-shelf bottom boundary layer. Ann. Rev. Fluid Mech., 18, 265-305.

Grant, W. D., A. J. Williams, III and S. M. Glenn, 1984: Bottom stress estimates and their prediction on the Northern California continental shelf during CODE-1: The importance of wave-current interaction. J. Phys. Oceanogr. 14, 506-527.

Inman, D. L., 1957: Wave generated ripples in nearshore sands. U. S. Army Corps of Engineers, Beach Erosion Board. TM-100, 42 pp.

Kajiura, K, 1968: A model of the bottom boundary layer in water waves. Bulletin of the Earthquake Research Institute, 46, 75-123.

Keen, T. R. and Glenn, S. M., 1994: A coupled hydrodynamic-bottom boundary layer model of Ekman flow on stratified continental shelves. J. Phys. Oceanogr., 24, 1733-1749.

Keen, T. R. and Glenn, S. M., 1995: A coupled hydrodynamic-bottom boundary layer model of storm and tidal flow in the Middle Atlantic Bight of North America. J. Phys. Oceanogr., 25, 391-406.

Keen, T. R. and Glenn, S. M., 1998: Factors influencing model skill for hindcasting shallow water currents during Hurricane Andrew. J. Atmos. Oceanic Technol., 15, 221-236.

Keen, T. R. and Slingerland, R. L., 1993a: A numerical study of sediment transport and event bed genesis during Tropical Storm Delia. J. Geophys. Res., 98, 4775-4791.

Keen, T. R. and Slingerland, R. L, 1993b: Four storm-event beds and the tropical cyclones that produced them: A numerical hindcast. J. Sed. Petrol., 63, 218-232.

Li, M. Z. and Amos, C. L., 1998: Predicting ripple geometry and bed roughness under combined waves and currents in a continental shelf environment. Cont. Shelf Res., 18, 941-970.

Lynch, J. F., Irish, J. D., Gross, T. F., Wiberg, P. L., Newhall, A. E., Traykovski, P. A. and Warren, J. D., 1997: Acoustic measurements of the spatial and temporal structure of the near-bottom boundary layer in the 1990-1991 STRESS experiment. Cont. Shelf Res., 17, 1271-1295.

Madsen, O. S. and Wikramanayake, P. N., 1991: Simple models for turbulent wave-current bottom boundary layer flow. U.S. Army Corps of Engineers, Coastal Engineering Research Center, Contract report DRP-91-1, 150 pp.

Madsen, O. S., 1994: Spectral wave-current bottom boundary layer flows. In: Proceedings of the 24th Coastal Engineering Conference, Kobe, 384-398.

Madsen, O. S., Wright, L. D., Boon, J. D. and Chisholm, T. A., 1993: Wind stress, bed roughness and sediment suspension on the inner shelf during an extreme storm event. Cont. Shelf Res., 13, 1303-1324.

Mathisen, P. P. and O. S. Madsen, 1995a: Waves and currents over a fixed rippled bed 1. Bottom roughness experienced by waves in the presence and absence of currents. J. Geophys. Res., 101, 16,533-16,542.

Mathisen, P. P. and O. S. Madsen, 1995b: Waves and currents over a fixed rippled bed 2. Bottom and apparent roughness experienced by currents in the presence of waves. J. Geophys. Res., 101, 16,543-16,550.

Miller, M. C. and Komar, P. D., 1980: A field investigation of the relationship between oscillation ripple spacing and the near-bottom water orbital motions. J. Sediment Petrol., 50, 183-191.

Nielsen, P., 1981: Dynamics and geometry of wave-generated ripples. J. Geophys., Res., 86, 6467-6472.

Nielsen, P., 1992: Coastal bottom boundary layers and sediment transport. World Scientific, 324 pp.

Signell, R. P., Beardsley, R. C., Graber, H. C. and Capotondi, A., 1990: Effect of wave-current interaction on wind-driven circulation in narrow, shallow embayments. J. Geophys. Res., 95, 9671-9678.

Sleath, J. F. A., 1991: Velocities and shear stresses in wave-current flows. J. Geophys. Res., 96, 15,237-15,244.

Smith, J. D., 1977: Modeling of sediment transport on continental shelves. The Sea, E. D. Goldberg, I. N. McCave, J. J. O'Brien, J. H. Steele, Eds., 6, Interscience, 538-577.

Spaulding, M. L. and Isaji, T. 1985: Design flow conditions near bottom, phase II, coupling of a continental shelf hydrodynamics model to a bottom boundary layer model. Vol. 1, Theoretical development and application. Final Rep. To Pipeline Res. Comm., Project PR-169-1186, Amer. Gas Assoc.

Styles, R., 1998: A continental shelf bottom boundary layer model: Development, calibration and applications to sediment transport in the Middle Atlantic Bight. Ph.D. thesis, Rutgers, The State Univ. of New Jersey, New Brunswick, 261 pp.

Styles, R. and Glenn, S. M., 2000: Modeling stratified wave and current bottom boundary layers on the continental shelf. J. Geophys. Res., 105, 24,119-14,139.

Traykovski, P., Hay, A. E., Irish, J. D. and Lynch, J. F., 1999: Geometry, migration, and evolution of wave orbital ripples at LEO-15. J. Geophys. Res., 104, 1505-1524.

Wiberg, P. and Smith, J. D., 1983: A comparison of field data and theoretical models for wave-current interactions at the bed on the continental shelf. Cont. Shelf Res., 2, 126-136.

Wiberg, P. 1995: A theoretical investigation of boundary layer flow and bottom shear stress for smooth, transitional, and rough flow under waves. J. Geophys. Res., 100, 22,667-22,679.